

The Transit Light Curve Project.

IV. Five Transits of the Exoplanet OGLE-TR-10b

Matthew J. Holman¹, Joshua N. Winn², Cesar I. Fuentes¹, Joel D. Hartman¹,
K. Z. Stanek³, Guillermo Torres¹, Dimitar D. Sasselov¹, B. Scott Gaudi^{1,3},
R. Lynne Jones⁴, Wesley Fraser⁵

ABSTRACT

We present I and B photometry of five distinct transits of the exoplanet OGLE-TR-10b. By modeling the light curves, we find the planetary radius to be $R_P = 1.06 \pm 0.08 R_{\text{Jup}}$ and the stellar radius to be $R_S = 1.10 \pm 0.07 R_{\odot}$. The uncertainties are dominated by statistical errors in the photometry. Our estimate of the planetary radius is smaller than previous estimates that were based on lower-precision photometry, and hence the planet is not as anomalously large as was previously thought. We provide updated determinations of all the system parameters, including the transit ephemerides.

Subject headings: planetary systems—stars: individual (OGLE-TR-10)—techniques: photometric

1. Introduction

Apart from Mercury and Venus, we know of 10 planets that transit their parent stars as viewed from Earth. Three of the transiting extrasolar planets (HD 209458b, HD 149026b, and HD 189733b) were discovered by observing radial velocity variations of the parent star and then searching for the photometric signal of transits (Mazeh et al. 2000; Charbonneau

¹Harvard-Smithsonian Center for Astrophysics, 60 Garden Street, Cambridge, MA 02138; mholman@cfa.harvard.edu

²Department of Physics, and Kavli Institute for Astrophysics and Space Research, Massachusetts Institute of Technology, Cambridge, MA 02139

³Department of Astronomy, The Ohio State University, Columbus, OH 43210

⁴National Research Council of Canada, Hertzberg Institute for Astrophysics, Victoria, BC, V9E 2E7, Canada

⁵Department of Physics and Astronomy, University of Victoria, Victoria, BC V8T 1Z1, Canada

et al. 2000; Henry et al. 2000; Sato et al. 2005; Charbonneau et al. 2005). In the other cases, the photometric signals were discovered first, and then confirmed as planetary transits through radial velocity studies (Udalski et al. 2002b,c,a, 2003, 2004; Bouchy et al. 2004, 2005; Konacki et al. 2003a,b, 2004, 2005; Alonso et al. 2004; Pont et al. 2004; McCullough et al. 2006). Regardless of the order of events, the combination of photometry and dynamical measurements allows the mass and radius of the planet (and hence its mean density) to be determined.

These measurements set the stage for a host of more subtle measurements of effects such as planetary atmospheric absorption lines, thermal emission, spin-orbit alignment, and timing anomalies, as reviewed recently by Charbonneau et al. (2006). They have also given us the first clues about the interior structures of these other worlds. Most of the transiting extrasolar planets have mean densities between 0.6 and 1.2 g cm⁻³, suggesting they are not too different from the well-studied gas giants Saturn (0.7 g cm⁻³) and Jupiter (1.3 g cm⁻³). However, the first transiting planet that was discovered, HD 209458b, has a much smaller density of 0.33 g cm⁻³ (Henry et al. 2000; Charbonneau et al. 2000; for the most recent analyses see Winn et al. 2005, Wittenmyer et al. 2005, and Knutson et al. 2006). This anomaly has led to speculation about novel sources of internal heat, such as eccentricity damping (Bodenheimer et al. 2001), insolation-driven weather patterns (Guillot & Showman 2002), and obliquity tides (Winn & Holman 2005).

The periodic dimming events of OGLE-TR-10 were discovered by Udalski et al. (2002b) in a survey for transiting planets in three star fields toward the Galactic center. Udalski et al. (2002a) reported additional observations that enabled the events to be predicted with greater precision. Spectroscopic follow-up observations by Konacki et al. (2005), in combination with those reported by Konacki et al. (2003b) and Bouchy et al. (2005), revealed a periodic Doppler shift and thereby confirmed that the dimming events were caused by the transits of a Jovian planet. The estimated planetary mass is $M_P = 0.57 \pm 0.12 M_\odot$. Because of the planet’s anomalously small mean density of 0.38 ± 0.10 g cm⁻³, the discovery of this system was greeted with considerable interest (Konacki et al. 2005; Bouchy et al. 2005; Baraffe et al. 2005; Laughlin et al. 2005; Gaudi 2005; Santos et al. 2006).

Through the recently initiated Transit Light Curve (TLC) Project, we are building a library of high-precision transit photometry, with the dual goals of (1) refining the estimates of the physical and orbital parameters of the target systems, and (2) searching for secular and short-term variations in the transit times and light curve shapes that would be indicative of perturbations from additional bodies (Agol et al. 2005; Holman & Murray 2005). We have previously reported on observations of the exoplanets XO-1b (Holman et al. 2006),

TrES-1 (Winn et al. 2006b), and OGLE-TR-111b (Winn et al. 2006a). In this paper¹, we present TLC results for OGLE-TR-10b. We describe our observations in § 2 and data reduction procedures in § 3. In § 4, we describe the modeling procedures by which we estimate the physical and orbital parameters of OGLE-TR-10. We present the results in § 5 and summarize our findings in § 6.

2. Observations and Data Reduction

We used the 6.5m Baade (Magellan I) and Clay (Magellan II) telescopes at Las Campanas Observatory, in northern Chile, to observe five different transits of OGLE-TR-10. These correspond to epochs $E = 223, 251, 252, 488$, and 597 of the ephemeris determined by Udalski et al. (2002c):

$$T_c(E) = 2,452,070.21900 \text{ [HJD]} + E \times (3.10140 \text{ days}). \quad (1)$$

We observed the first four transits with the Raymond and Beverly Sackler Magellan Instant Camera (MagIC) on the Clay telescope. MagIC is a $2k \times 2k$ SITe back-illuminated and thinned CCD with $24 \mu\text{m}$ pixels. For transits $E = 223, 251$, and 252, we alternated between observations in Johnson-Cousins B and I filters. For transit $E = 488$, we used the I filter only. We used a typical exposure time of 30-60 s. The readout and reset time was about 25 s and the read noise was about $5 \text{ e}^- \text{ pixel}^{-1}$. The seeing varied from $0.4\text{--}2''$.

A low-amplitude herringbone pattern was evident in the MagIC images. The same pattern appeared in each of the 4 quadrants of an individual exposure, but the pattern varied randomly between images. This is a known problem resulting from 60 Hz noise. For each image, we created a herringbone template by taking the median of the four quadrants after masking the stars and applying a narrow-band 60 Hz Fourier filter, based on an algorithm kindly provided by S. Burles. We then subtracted the isolated and purified herringbone pattern from the images. A shutter correction was applied, and bad pixels were assigned values based on linear interpolation of neighboring pixel values.

We observed the fifth transit ($E = 597$) with the Inamori Magellan Areal Camera and Spectrograph (IMACS) on the Baade telescope. The IMACS detector is a mosaic of eight $2k \times 4k$ SITe back-illuminated and thinned CCDs with $15 \mu\text{m}$ pixels. We used the “long”

¹This paper is a thorough revision of (and supersedes) a previous version of this manuscript that was circulated on astro-ph in 2005. The most important change is that we obtained observations of 2 additional full transits to check our results. The new data are in agreement with our original data, and our conclusion is unchanged that the planetary radius is smaller than was previously believed. See § 5 for a discussion.

($f/4.3$) camera, giving a pixel scale of $0''.111$ and a field of view of $15''.4$. To reduce the readout time, we read only one third of each chip, corresponding to the central $15''.4 \times 5''.1$ of the mosaic. The readout time was approximately 45 s and the readout noise was about 5 e^- . We observed through the CTIO I band filter.

All of the images, from both MagIC and IMACS, were overscan corrected, trimmed, and divided by a flat-field image with standard IRAF² routines. A bias frame was subtracted from the IMACS images before the flat-field correction was applied (this step was unnecessary for the MagIC images). We obtained the dome flat exposures and zero-second (bias) exposures at the beginning of each night.

Because the region surrounding OGLE-TR-10 was too crowded for aperture photometry, we used the method of image subtraction as implemented by Alard & Lupton (1998) and Alard (2000). Specifically, we used version 2.2 of the ISIS image subtraction package that was written and kindly made public by C. Alard. In this method, all of the images from a given night are registered to a common pixel frame, and a reference image is created by combining a subset ($\approx 10\%$) of the images with the best seeing from that night. For each individual image, a convolution kernel is determined that brings the image into best agreement with the reference image. Then the difference between the appropriately convolved image, and the reference image, is computed. The advantage of this method is that photometry is simplified on the difference images, because most stars are not variable stars and thus the complex and crowded background is eliminated. It is still necessary to compute the flux of the variable stars on the reference image, taking into account any neighboring stars, but this need only be done once, and the task is facilitated by the good spatial resolution and high signal-to-noise ratio of the reference image. Thus, the measurement of the relative flux $f(t)$ takes the form

$$f(t) = [f_{\text{ref}} + \Delta f(t)] / f_{\text{out}}, \quad (2)$$

where f_{ref} is measured on the reference image, $\Delta f(t)$ is measured on the difference images, and f_{out} is the out of transit flux. We derived f_{ref} for each of the reference images by using DAOPHOT (Stetson 1987) to measure the flux through a small aperture with PSF fitting, and then calculating the appropriate aperture correction by examining an ensemble of bright, relatively isolated stars for which we had subtracted any remaining nearby stars.

Although the image subtraction method removes the first-order effects of extinction by scaling all of the images to a common flux level before subtraction, residual color-dependent

²IRAF is distributed by the National Optical Astronomy Observatories, which are operated by the Association of Universities for Research in Astronomy, Inc., under cooperative agreement with the National Science Foundation.

effects are not removed. Stars of different colors are extinguished by different amounts through a given airmass z . Thus, as part of the fitting procedure discussed in § 3, we apply a residual extinction correction to the data such that the observed flux is proportional to $\exp(-kz)$, where k is a residual extinction coefficient.

The uncertainty in the each data point arises from two sources: the uncertainty in the difference flux Δf , and the uncertainty in the reference flux f_{ref} . We estimated the uncertainty in the difference flux based on Poisson statistics. This turned out to be an underestimate; some correlated errors are evident in the final light curves (see the next section). We estimated the uncertainty in the reference flux based not only on Poisson statistics, but also by the spread in the values obtained when using different choices for the stars used to determine the point-spread-function (PSF) and other parameters relating to the profile photometry. This latter source of systematic error was typically 1%, which dominated the Poisson error in the reference flux determination. However, adjustments in f_{ref} affect all of the points from a given night in the same way; the net effect is a small modification of the transit depth. For example, for OGLE-TR-10 the transit depth is approximately 1%. Because $f_{\text{out}} \sim f_{\text{ref}}$, the effect of increasing f_{ref} by 1% is to decrease the transit depth by (0.01×0.01) or 10^{-4} . As we will show in the next section, this error proved to be smaller than the other errors in the difference fluxes. In addition, there may be a systematic error of order 3 seconds (3×10^{-5} days) in the reported observation times, due to a delay between the opening of the shutter and the recording of the time. We have not verified or attempted to correct for this delay.

3. The Model

Of the five nights of observations, the data from the two most recent events ($E = 488$ and 597) have the highest sampling frequency and most uniform coverage and quality. We determined the system parameters of OGLE-TR-10b by fitting a model to these data only. Our model and fitting algorithm are similar to those employed in previous TLC papers (Holman et al. 2006; Winn et al. 2006a,b). The model posits a circular Keplerian orbit of a star with mass M_S and radius R_S , and a planet with mass M_P and radius R_P with period P and inclination i relative to the sky plane³. We define the coordinate system such that $0^\circ \leq i \leq 90^\circ$.

³Unless there is positive evidence for a nonzero eccentricity, a circular orbit is a reasonable simplifying assumption for a “hot Jupiter” around a main-sequence star. This is because (in the absence of any third body) it is expected that there has been sufficient time for tides to have damped out any initial eccentricity, in the absence of a third body (see, e.g., Rasio et al. 1996; Trilling 2000; Dobbs-Dixon et al. 2004).

The stellar mass cannot be determined from transit photometry alone. There is a well-known degeneracy among M_S , R_S and R_P that prevents all three parameters from being uniquely determined from transit photometry alone, unless a stellar mass-radius relation is assumed (Seager & Mallén-Ornelas 2003). Our approach was to fix $M_S = 1.025^{+0.135}_{-0.130} M_\odot$ based on an analysis of the stellar spectrum (see the discussion in § 4). We then use the scaling relations $R_P \propto M_S^{1/3}$ and $R_S \propto M_S^{1/3}$ to estimate the systematic error due to the uncertainty in M_S . The planetary mass M_P is irrelevant to the model except for its minuscule effect on the relation between P and the semimajor axis; for completeness, we assume $M_P = 0.57 \pm 0.12 M_\odot$, the value reported by Konacki et al. (2005).

We allow each of the two fitted transits to have an independent value of T_c , the transit midpoint, rather than forcing them to be separated by an integral number of orbital periods. Thus, the period P is relevant to the model only through the connection between the total mass and the orbital semimajor axis. We fix $P = 3.10140$ days (Udalski et al. 2002a).

The model flux is unity outside of transit, and is otherwise computed using a quadratic limb darkening law, $I = 1 - u_1(1 - \mu) - u_2(1 - \mu)^2$. We employed the analytic formulas of Mandel & Agol (2002) to compute the integral of the intensity over the exposed portion of the stellar disk. We allow the photometry of each night (and in each filter) to have an independent out of transit flux f_{out} and residual extinction coefficient k . We hold the limb darkening parameters fixed at $u_1 = 0.2541$, $u_2 = 0.3254$ in I , as appropriate for a star with the assumed properties⁴ and a microturbulent velocity of 2 km s^{-1} (Claret 2000).

In total, there are 9 adjustable parameters describing $N_f = 601$ photometric data points. The parameters are R_S , R_P , and i ; the two values of T_c ; and the values of f_{out} and k for each transit. The goodness-of-fit parameter is

$$\chi^2 = \sum_{j=1}^{N_f} \left[\frac{f_j(\text{obs}) - f_j(\text{calc})}{\sigma_j} \right]^2 \quad (3)$$

where $f_j(\text{obs})$ is the flux observed at time j , σ_j is the corresponding uncertainty, and $f_j(\text{calc})$ is the calculated value.

First we use an AMOEBA algorithm (Press et al. 1992) to identify the parameter values that minimize χ^2 . We then rescale the uncertainties σ_j by a factor that is specific to each of the two time series, such that $\chi^2/N_{\text{DOF}} = 1$ for each time series individually. Then

⁴There is a systematic error associated with the uncertainty in the limb darkening function, but it is probably much smaller than the other sources of error. For example, if we adopt the coefficients that are appropriate to the hotter star favored by Bouchy et al. (2005) and Santos et al. (2006), our inferred values of R_P and R_S change by about 1.5%, which can be neglected in comparison to the 6% statistical errors.

we estimate the *a posteriori* joint probability distribution for the parameter values using a Markov Chain Monte Carlo (MCMC) technique (see, e.g., Tegmark et al. 2004). In this method, a chain of points in parameter space is generated from an initial point by iterating a jump function, which in our case was the addition of a Gaussian random number to each parameter value. If the new point has a lower χ^2 than the previous point, the jump is executed; if not, the jump is only executed with probability $\exp(-\Delta\chi^2/2)$. We set the typical sizes of the random perturbations such that $\sim 20\%$ of jumps are executed. We created 10 independent chains, each with 500,000 points, starting from random initial positions. The first 100,000 points were not used, to minimize the effect of the initial condition. The Gelman & Rubin (1992) R statistic was within 0.5% of unity for each parameter, a sign of good mixing and convergence.

Next we verify that our *BI* photometry of events $E = 223, 251$, and 252 (for which the time coverage was sparser) is consistent with the model parameters derived above. We fix the stellar and planetary radii, inclination, and period at the best fit values. We hold the limb-darkening coefficients fixed as before (with $u_1 = 0.6385$, $u_2 = 0.1789$ in B). We vary only the values of f_{tot} and k for each of the time series, as well as the three independent values of T_c . The final photometry is given in Table 1, and is plotted in Figs. 1 and 2. For comparison, the OGLE light curve is shown in Fig. 3. The uncertainties given in Table 1 are the uncertainties in the difference fluxes, after multiplying by a factor specific to each night such that $\chi^2/N_{\text{DOF}} = 1$ for the best-fitting model. The data from individual transits are all generally consistent with one another. Systematic errors are evident, especially in the $E = 251$ data, but by fitting for the residual extinction correction we have taken into account the main systematic error that would afflict the determination of T_c .

4. The Results

The model that minimizes χ^2 is plotted as a solid line in Figs. 1-3. The optimized residual extinction correction has been applied to the data that are plotted in Fig. 1, and to the data that are given in Table 1. The differences between the observed fluxes and the model fluxes are also shown beneath each light curve. Table 2 gives the estimated values and uncertainties for each parameter based on the MCMC analysis. It also includes some useful derived quantities: the impact parameter $b = a \cos i / R_S$ (where a is the semimajor axis); the time between first and last contact ($t_{\text{IV}} - t_{\text{I}}$); and the time between first and second contact ($t_{\text{II}} - t_{\text{I}}$). Fig. 4 shows the estimated *a posteriori* probability distributions for the especially interesting parameters R_S , R_P and b , along with some of the two-dimensional correlations involving those parameters. Although the distributions shown in Fig. 4 are

somewhat asymmetric about the median, Table 2 reports only the median p_{med} and a single number σ_p characterizing the width of the distribution. The value of σ_p is the average of $|p_{\text{med}} - p_{\text{hi}}|$ and $|p_{\text{med}} - p_{\text{lo}}|$, where p_{lo} and p_{hi} are the lower and upper 68% confidence limits.

Our estimate of the planetary radius, $R_P = 1.06 \pm 0.08 R_{\text{Jup}}$, is smaller than the previous estimates of $R_P/R_{\text{Jup}} = 1.24 \pm 0.09$ (Konacki et al. 2005) and 1.54 ± 0.12 (Bouchy et al. 2004), both of which were based on the OGLE discovery photometry. It is important to note that both of these earlier works used a value for R_S that was determined from an analysis of the stellar spectrum, whereas we have determined R_S by fitting the transit light curves. One reason that the previous estimates of the planetary radius were larger is the apparently larger value of the flux decrement in the OGLE photometry (see Fig. 1). The larger discrepancy with Bouchy et al. (2004) is also due to their assumption of a larger value for the stellar radius.

We do not know why the OGLE photometry shows a larger decrement. We first saw this discrepancy based on our 2003 data (which was the basis of an earlier version of this manuscript that was circulated on astro-ph). We could not find any errors in our photometry, but because none of our light curves adequately covered a complete transit we decided to obtain additional photometry in 2005 and 2006 to try to resolve the matter. The transit depth in the newer and more complete light curves is also shallower than in the OGLE light curve, and is in agreement with our earlier data, despite differences in the telescope, detector and observing conditions. Although there are systematic errors in both our photometry and the OGLE photometry (see Figs. 1 and 2), one would expect our data to be more trustworthy, since they are of higher precision and more frequent sampling. We also note that of the seven transits of OGLE-TR-10 observed by OGLE, only two (JD 2452085 and 2452113) were observed for a complete transit including both pre-ingress and post-egress data. Such data allow one to visually check for systematic errors that might affect the measured transit depth (which is why we obtained the two additional light curves in 2005 and 2006). The full transit on JD 2452085 is shallower than the best model of Konacki et al. (2005), and the pre-ingress observations on JD 2452113 are fainter than those post-egress. The OGLE team has consistently provided outstanding survey data, but the data are necessarily reduced through a bulk photometry pipeline, as opposed to the individual attention we have lavished on OGLE-TR-10. Hence we proceed under the assumption that our photometry is correct. A full resolution of this discrepancy would probably require revisiting the original OGLE image frames.

Another point of disagreement regarding this system is the choice of the stellar mass, which must be made independently of the transit photometry. Estimates of the stellar mass are based on analyses of the stellar spectrum. First, the values of T_{eff} , $\log g$, and metallicity

are estimated by measuring the equivalent widths and profiles of appropriate lines and comparing them to stellar-atmosphere models. Then, these derived parameters are converted into a stellar mass, radius, and age, with reference to theoretical models of stellar evolution (“isochrones”).

The two panels of figure 6 show Yonsei-Yale isochrones (Yi et al. 2003) for two respective metallicities of OGLE-TR-10. The left panel shows isochrones for the metal-rich value measured by Santos et al. (2006); the right panel shows isochrones assuming solar metallicity. Santos et al. (2006), whose results supercede those of Bouchy et al. (2005), measure an effective temperature $T_{\text{eff}} = 6075 \pm 86$ K and a surface gravity $\log g = 4.54 \pm 0.15$. These are indicated by the shaded rectangle. The red line shows the isochrone that best matches their results, without passing below the ZAMS. It is clear that this isochrone is only marginally consistent with their estimates of the effective temperature and surface gravity. In addition, the best fitting isochrone corresponds to a very young stellar age of 0.2 Gyr. Thus, we have re-analyzed the spectra of Konacki et al. (2005). We confirm the measurement of solar metallicity $[\text{Fe}/\text{H}] = 0.0 \pm 0.2$. We also confirm $\log g = 4.4^{+0.3}_{-0.7}$ and a slightly higher $T_{\text{eff}} = 5800 \pm 100$ K. We made wider use of temperature sensitive pairs of metal lines in deriving the effective temperature (after Gray & Johanson 1991). We used the following lines: VI 625.183 and FeI 625.257 nm, SiI 612.503 and TiI 612.622 nm, VI 615.015 and FeI 615.162 nm. All three pairs gave consistent results. In addition, we estimated $v \sin i = 3 \pm 1$ km/sec, with microturbulent velocity of 1.0 km/sec and adopted (for this T_{eff}) macroturbulent broadening of 3.5 km/sec. In analogy to the planetary system HD 209458, we assume that $v \sin i$ of a star with a transiting hot Jupiter is equal to the rotational velocity v_{rot} . This allows us to constrain the upper bound of the star’s luminosity on the HR diagram, by using an empirical relation between stellar age and rotation (Pace & Pasquini 2004). The larger the rotational velocity of a G0 dwarf, the younger and closer to the ZAMS it has to be. This constraint eliminates high luminosities (and subgiant models) that are otherwise allowed for OGLE-TR-10, due to the inability to constrain $\log g$ with sufficient accuracy with the spectra. In addition, the luminosity can be constrained from below, as models below the ZAMS of $[\text{Fe}/\text{H}] = -0.2$ are excluded as well. These constraints, converted back to $\log g$ in order to aid the illustration, are displayed in the right panel of Fig. 6. The red line in the right panel shows the isochrone that best fits the constraints on T_{eff} , $\log g$, and $[\text{Fe}/\text{H}]$. This isochrone corresponds to a 5.0 Gyr stellar age. This consistency gives us confidence in our measurements of effective temperature and surface gravity. We find the corresponding stellar mass to be $M_S = 1.025^{+0.125}_{-0.120} M_{\odot}$. To this should be added a systematic error of $\sim 0.05 M_{\odot}$ due to the unknown helium abundance and convective mixing-length parameter. The theoretical radius estimate is $R_S/R_{\odot} = 1.057^{+0.194}_{-0.160}$.

Fortunately, the fitted radius estimates depend weakly on the stellar mass. As explained

in § 3, our procedure was to assume $M_S/M_\odot = 1.025$ and allow the stellar radius to be a free parameter. The result was $R_S = 1.10 \pm 0.07 R_\odot$, which is consistent with the theoretical value above. If we assume the Santos et al. (2006) value of the stellar mass, $M_S/M_\odot = 1.17$, we find $R_S = 1.151 \pm 0.065 R_\odot$, which is also consistent with both the theoretical value determined by Santos et al. (2006), $R_S = 1.144 \pm 0.062 R_\odot$, as well as with our value. The larger value of the stellar mass also has negligible effect on the estimate of the planetary radius: $R_P = 1.103 \pm 0.075 R_{\text{Jup}}$ in comparison to the value $R_P = 1.06 \pm 0.08 R_{\text{Jup}}$ determined with our mass estimate. Although a more accurate determination of the stellar mass would be necessary to take full advantage of higher precision photometry, such as that obtained with the HST, it is not needed for this work.

We fitted a straight line to the transit times (T_c) listed in Table 2 to derive a new ephemeris

$$T_c(E) = 2453921.684(1) \text{ HJD} + E \times 3.101278(4) \text{ days}, \quad (4)$$

where the numbers in parentheses are the 1σ uncertainties in the final quoted digits. Evaluating the dynamical significance of the transit times, as was done for TrES-1 by Steffen & Agol (2005) and for HD 209458b by Miller-Ricci et al. (2005), is left for a future investigation.

5. Discussion

Our results provide further evidence that the transits of OGLE-TR-10 are caused by a short-period planetary companion. The light curves have a flat bottom, a feature that is inconsistent with most of the alternative hypotheses involving blends of an eclipsing binary. As further evidence against a blend, OGLE-TR-10 appears unresolved even in the images with the best seeing ($0''.4$).

It was previously thought that OGLE-TR-10b has a radius that is significantly larger than predicted by models of strongly irradiated gas giants. This would make it similar to the first-discovered transiting planet HD 209458b, perhaps heralding a new subclass of planets that share a mysterious internal heating mechanism. The suggestion that OGLE-TR-10 is anomalously large was made by Konacki et al. (2005) and was supported with calculations by Baraffe et al. (2005) and Laughlin et al. (2005), who found that the measured radii of all the transiting planets could be easily explained except for HD 209458b and OGLE-TR-10. Likewise, Gaudi (2005) derived radii of $1.04 R_{\text{Jup}}$ and $1.18 R_{\text{Jup}}$ for OGLE-TR-10 with and without a core, respectively, from the models presented in Bodenheimer et al. (2003). These estimates include a 5% increase to account for the effect pointed out by Burrows et al. (2003), that the measured radius of a transiting planet refers to the scale height of the planetary atmosphere at which the stellar flux encounters optical depth ~ 1 in the direction toward

the observer. Our results indicate that OGLE-TR-10b does not have an anomalously large radius, and that its radius is indeed consistent with standard structural models.

We are grateful to S. Burles for sharing his algorithm for Fourier filtering of MagIC images. W.F. thanks the SAO Summer Intern Program. M.J.H. and R.L.A. acknowledge support from STScI grants GO 9433.05 and GO 9433.06. Work by J.N.W. was supported by NASA through grant HST-HF-01180.02-A. Work by G.T. was supported by NASA Origins grant NNG04GL89G.

REFERENCES

- Agol, E., Steffen, J., Sari, R., & Clarkson, W. 2005, MNRAS, 359, 567
- Alard, C. 2000, A&AS, 144, 363
- Alard, C. & Lupton, R. H. 1998, ApJ, 503, 325
- Alonso, R. et al. 2004, ApJ, 613, L153
- Baraffe, I., Chabrier, G., Barman, T. S., Selsis, F., Allard, F., & Hauschildt, P. H. 2005, A&A, 436, L47
- Bodenheimer, P., Laughlin, G., & Lin, D. N. C. 2003, ApJ, 592, 555
- Bodenheimer, P., Lin, D. N. C., & Mardling, R. A. 2001, ApJ, 548, 466
- Bouchy, F., Pont, F., Melo, C., Santos, N. C., Mayor, M., Queloz, D., & Udry, S. 2005, A&A, 431, 1105
- Bouchy, F., Pont, F., Santos, N. C., Melo, C., Mayor, M., Queloz, D., & Udry, S. 2004, A&A, 421, L13
- Burrows, A., Sudarsky, D., & Hubbard, W. B. 2003, ApJ, 594, 545
- Charbonneau, D. et al. 2005, ApJ, 626, 523
- Charbonneau, D., Brown, T. M., Burrows, A., & Laughlin, G. 2006, in *Protostars & Planets V*, ed. B. Reipurth, D. Jewitt, & K. Keil (Tucson: University of Arizona Press), in press, astro-ph/0603376
- Charbonneau, D., Brown, T. M., Latham, D. W., & Mayor, M. 2000, ApJ, 529, L45

- Claret, A. 2000, *A&A*, 363, 1081
- Dobbs-Dixon, I., Lin, D. N. C., & Mardling, R. A. 2004, *ApJ*, 610, 464
- Gaudi, B. S. 2005, *ApJ*, 628, L73
- Gelman, A. & Rubin, D. B. 1992, *Stat. Sci.*, 7, 457
- Gray, D. F. & Johanson, H. L. 1991, *PASP*, 103, 439
- Guillot, T. & Showman, A. P. 2002, *A&A*, 385, 156
- Henry, G. W., Marcy, G. W., Butler, R. P., & Vogt, S. S. 2000, *ApJ*, 529, L41
- Holman, M. J. & Murray, N. W. 2005, *Science*, 307, 1288
- Holman, M. J. et al. 2006, *ArXiv:astro-ph/0607571*
- Knutson, H., Charbonneau, D., Noyes, R. W., Brown, T. M., & Gilliland, R. L. 2006, *ArXiv:astro-ph/0603542*
- Konacki, M., Torres, G., Jha, S., & Sasselov, D. D. 2003a, *Nature*, 421, 507
- Konacki, M., Torres, G., Sasselov, D. D., & Jha, S. 2003b, *ApJ*, 597, 1076
- . 2005, *ApJ*, 624, 372
- Konacki, M. et al. 2004, *ApJ*, 609, L37
- Laughlin, G., Wolf, A., Vanmunster, T., Bodenheimer, P., Fischer, D., Marcy, G., Butler, P., & Vogt, S. 2005, *ApJ*, 621, 1072
- Mandel, K. & Agol, E. 2002, *ApJ*, 580, L171
- Mazeh, T. et al. 2000, *ApJ*, 532, L55
- McCullough, P. R. et al. 2006, *ArXiv:astro-ph/0605414*
- Miller-Ricci, E. et al. 2005, *Bulletin of the American Astronomical Society*, 37, 1339
- Pace, G. & Pasquini, L. 2004, *A&A*, 426, 1021
- Pont, F., Bouchy, F., Queloz, D., Santos, N. C., Melo, C., Mayor, M., & Udry, S. 2004, *A&A*, 426, L15

- Press, W. H., Teukolsky, S. A., Vetterling, W. T., & Flannery, B. P. 1992, Numerical recipes in C. The art of scientific computing (Cambridge: University Press, —c1992, 2nd ed.)
- Rasio, F. A., Tout, C. A., Lubow, S. H., & Livio, M. 1996, *ApJ*, 470, 1187
- Santos, N. C. et al. 2006, *A&A*, 450, 825
- Sato, B. et al. 2005, *ApJ*, 633, 465
- Seager, S. & Mallén-Ornelas, G. 2003, *ApJ*, 585, 1038
- Steffen, J. H. & Agol, E. 2005, *MNRAS*, 364, L96
- Stetson, P. B. 1987, *PASP*, 99, 191
- Tegmark, M. et al. 2004, *Phys. Rev. D*, 69, 103501
- Trilling, D. E. 2000, *ApJ*, 537, L61
- Udalski, A., Szewczyk, O., Zebrun, K., Pietrzynski, G., Szymanski, M., Kubiak, M., Soszynski, I., & Wyrzykowski, L. 2002a, *Acta Astronomica*, 52, 317
- Udalski, A., Pietrzynski, G., Szymanski, M., Kubiak, M., Zebrun, K., Soszynski, I., Szewczyk, O., & Wyrzykowski, L. 2003, *Acta Astronomica*, 53, 133
- Udalski, A., Szymanski, M. K., Kubiak, M., Pietrzynski, G., Soszynski, I., Zebrun, K., Szewczyk, O., & Wyrzykowski, L. 2004, *Acta Astronomica*, 54, 313
- Udalski, A., Zebrun, K., Szymanski, M., Kubiak, M., Soszynski, I., Szewczyk, O., Wyrzykowski, L., & Pietrzynski, G. 2002c, *Acta Astronomica*, 52, 115
- Udalski, A. et al. 2002b, *Acta Astronomica*, 52, 1
- Winn, J. N. & Holman, M. J. 2005, *ApJ*, 628, L159
- Winn, J. N., Holman, M. J., & Fuentes, C. 2006a, *AJ*, submitted
- Winn, J. N., Holman, M. J., & Roussanova, A. 2006b, *ApJ*, submitted
- Winn, J. N. et al. 2005, *ApJ*, 631, 1215
- Wittenmyer, R. A. et al. 2005, *ApJ*, 632, 1157
- Yi, S. K., Kim, Y.-C., & Demarque, P. 2003, *ApJS*, 144, 259

Table 1. Photometry of OGLE-TR-10

Instrument	Filter	HJD	Relative flux	Uncertainty
IMACS	<i>I</i>	2453921.58279	1.00140	0.00247

Note. — The time stamps represent the Heliocentric Julian Date at the time of mid-exposure. The uncertainty estimates are based on the procedures described in § 2. We intend for this table to appear in entirety in the electronic version of the journal. A portion is shown here to illustrate its format. The data are also available from the authors upon request.

Table 2. System parameters of OGLE-TR-10

Parameter	Value	Stat. Error	Sys. Error due to M_S	Total Error
R_S/R_\odot	1.095	0.055	0.048	0.073
R_P/R_{Jup}	1.056	0.069	0.046	0.083
R_P/R_S	0.0990	0.0021
i [deg]	88.1	1.2
b	0.28	0.17
$t_{\text{IV}} - t_{\text{I}}$ [hr]	3.072	0.050
$t_{\text{II}} - t_{\text{I}}$ [min]	17.9	2.0
$T_c(597)$ [HJD]	2453921.68315	0.00056
$T_c(488)$ [HJD]	2453583.64572	0.00053
$T_c(252)$ [HJD]	2452851.74563	0.00064
$T_c(251)$ [HJD]	2452848.64208	0.00043
$T_c(223)$ [HJD]	2452761.80544	0.00091

Note. — The parameter values in Column 2 are the median values p_{med} of the MCMC distributions. The statistical error given in Column 3 is the average of $|p_{\text{med}} - p_{\text{lo}}|$ and $|p_{\text{med}} - p_{\text{hi}}|$, where p_{lo} and p_{hi} are the lower and upper 68% confidence limits. These results are based upon the assumption $M_S/M_\odot = 1.025$ exactly. The error given in Column 4 is the additional systematic error due to the covariance with the stellar mass, which was taken to be $M_S = 1.025^{+0.135}_{-0.130} M_\odot$. Column 5 shows the quadrature sum of the statistical and systematic errors for the stellar and planetary radii.

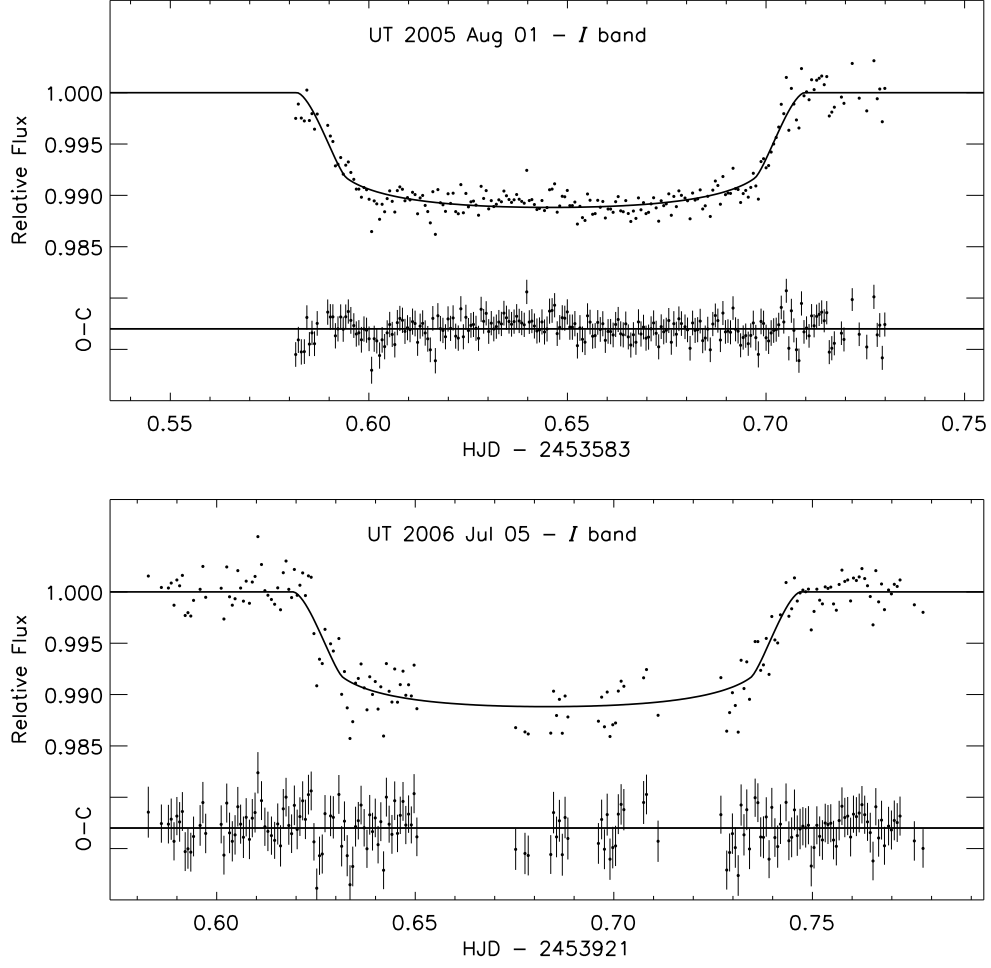


Fig. 1.— Relative I photometry of OGLE-TR-10 during the $E = 488$ and 597 transits. The panels show the photometry (points) and the best-fitting model (solid line), along with the residuals (observed – calculated). These two data sets were the ones used to determine the OGLE-TR-10 system parameters because they had the best time sampling and accuracy.

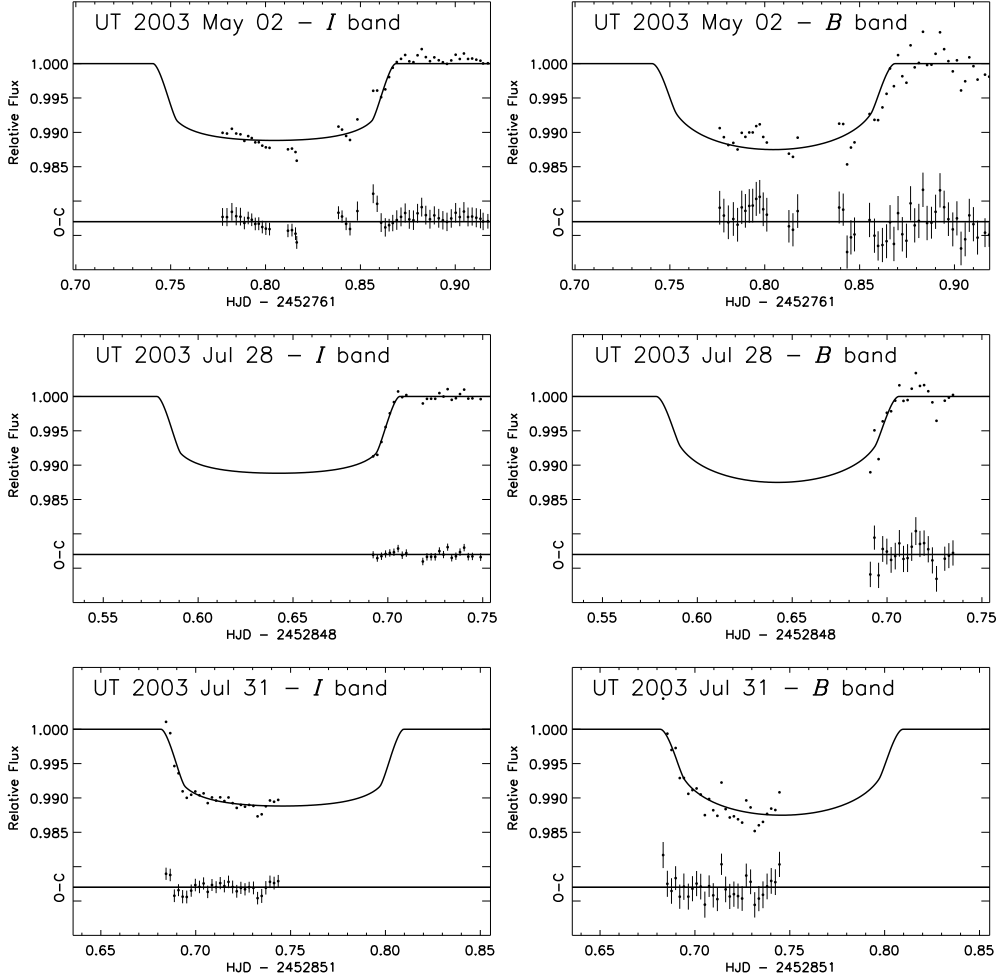


Fig. 2.— Relative *BI* photometry of OGLE-TR-10 during the $E = 223$, 251, and 252 transits. The panels show the photometry (points) and the best-fitting model (solid line), along with the residuals (observed – calculated). These data sets had incomplete coverage of the transits and were used only as a consistency check and to estimate transit midpoint times.

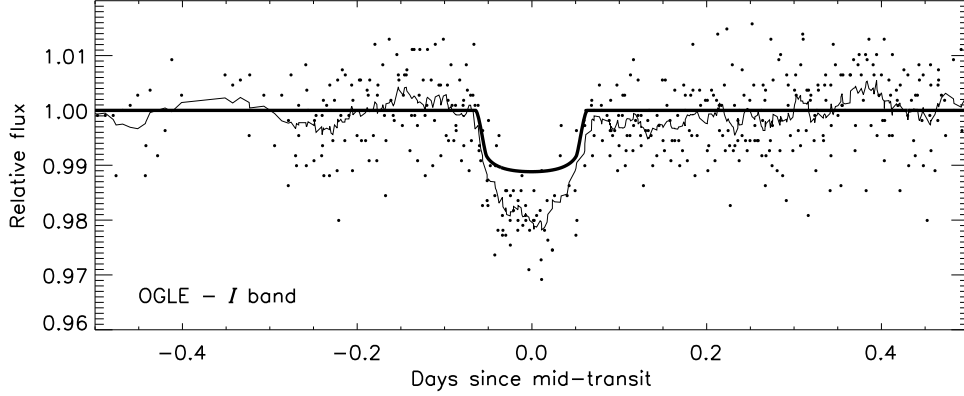


Fig. 3.— Relative I photometry of OGLE-TR-10, from the OGLE discovery and follow-up data (Udalski et al. 2002ac). The photometry (points) and our best-fitting model (solid line) are plotted, showing that our model has a shallower transit. The jagged line is a boxcar-smoothed version of the data (with a boxcar size of 10 points), giving a visual cue of the 0.5% correlated errors in the OGLE photometry.

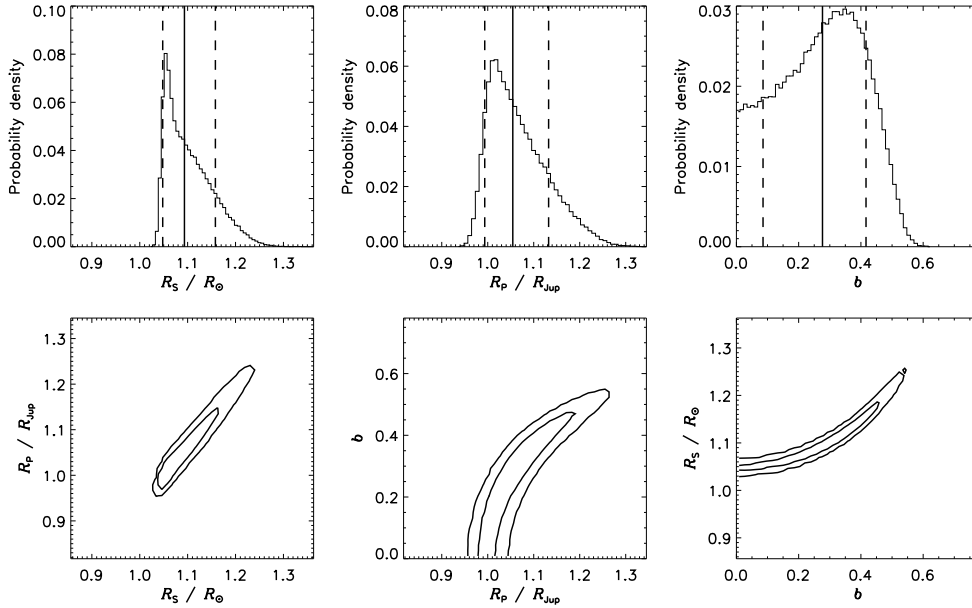


Fig. 4.— **Top row.** Probability distributions for the stellar radius R_S , planetary radius R_P , and impact parameter $b \equiv a \cos i / R_S$, based on the MCMC simulations. The solid lines mark the median values; the dashed lines mark the 68% confidence limits. **Bottom row.** Joint probability distributions of those parameters with the strongest correlations. The contours are isoprobability contours enclosing 68% and 95% of the points in the Markov chains.

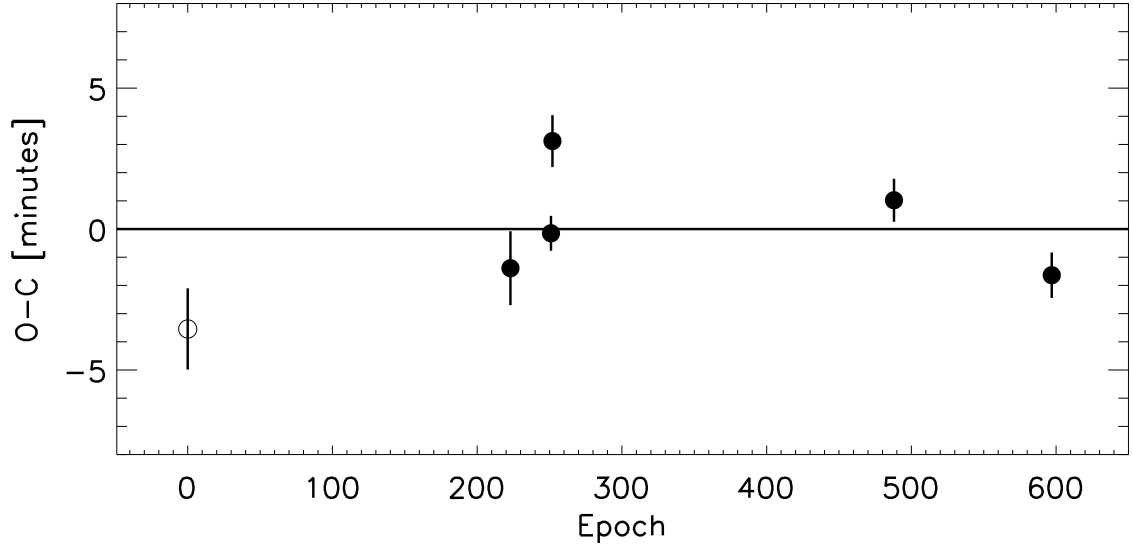


Fig. 5.— Transit timing residuals for OGLE-TR-10. The calculated transit times have been subtracted from the observed transit times. The open symbol indicates the T_c from Udalski et al. (2002a); we estimate its uncertainty to be 0.001 days. The solid symbols indicate our measurements. The best-fitting line is plotted, representing the updated ephemeris given in Eq. 4 and the text that follows it.

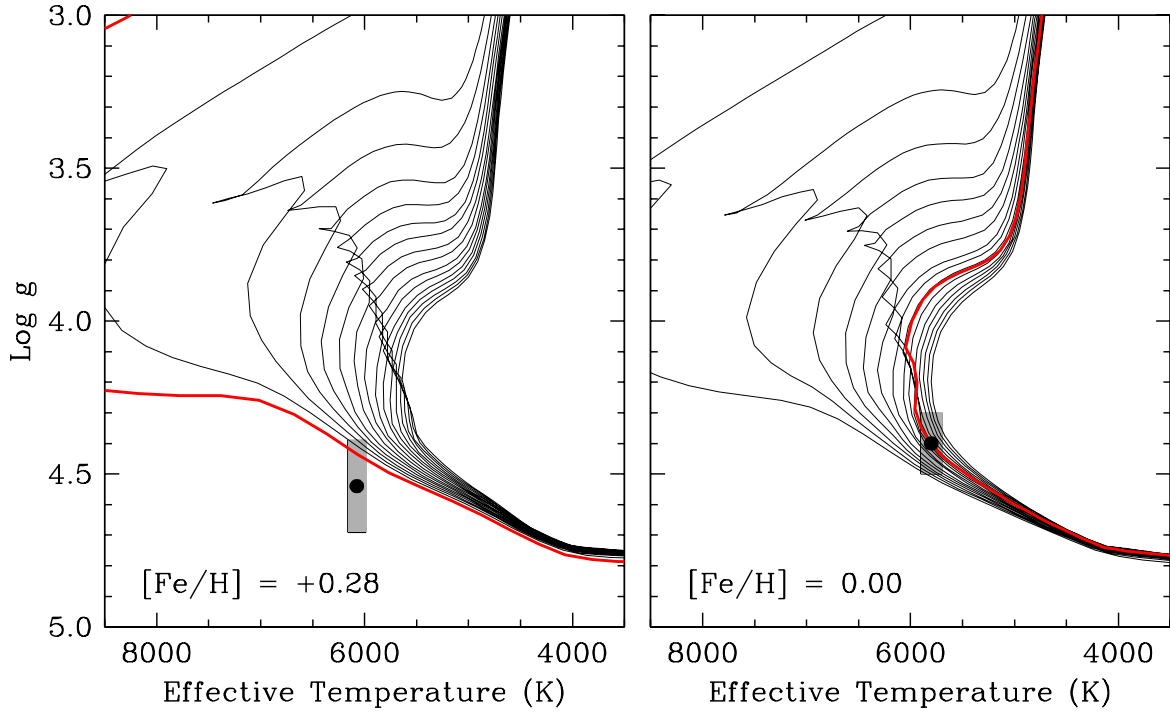


Fig. 6.— Yonsei-Yale isochrones as a function of effective temperature and surface gravity (Yi et al. 2003). **Left.** Isochrones for the metallicity determined by Santos et al. (2006). The black point marks the best-fit effective temperature and surface gravity measured in that work. The shaded rectangle indicates the uncertainties in effective temperature and surface gravity. The red line shows the isochrone that best fits the constraints on T_{eff} , $\log g$, and $[\text{Fe}/\text{H}]$, without passing below the ZAMS. It corresponds to a stellar age of 0.2 Gyr and a metal content $[\text{Fe}/\text{H}] = 0.18$. **Right.** Corresponding isochrones for solar metallicity, as determined by Konacki et al. (2005) and by this work. The red line corresponds to a stellar age of 5.0 Gyr and a metallicity $[\text{Fe}/\text{H}] = 0.04$.